University of Nebraska - Lincoln

DigitalCommons@University of Nebraska - Lincoln

West Central Research and Extension Center,
North Platte

Agricultural Research Division of IANR

2023

Measuring and preliminary modeling of drift interception by plant species

Jonnie B. Dunne

Shanique L. Grant

Jeffrey A. Golus

Jeffrey W. Perine

Stefan Wolf

See next page for additional authors

Follow this and additional works at: https://digitalcommons.unl.edu/westcentresext

Part of the Agriculture Commons, Ecology and Evolutionary Biology Commons, and the Plant Sciences Commons

Authors

Jonnie B. Dunne, Shanique L. Grant, Jeffrey A. Golus, Jeffrey W. Perine, Stefan Wolf, Michael Winchell, T. Mark Ledson, and Ian Whenham

TECHNICAL REPORT

Ecological Risk Assessment

Measuring and preliminary modeling of drift interception by plant species

Jonnie B. Dunne[1] | **Shanique L. Grant**[2] | **Jeffrey A. Golus**[3] | **Jeffrey W. Perine**[2] | **Stefan Wolf**[4] | **Michael Winchell**[1] | **T. Mark Ledson**[2] | **Ian Whenham**[5]

[1]Stone Environmental, Montpelier, USA

[2]Syngenta Crop Protection, Greensboro, USA

[3]West Central Research and Extension Center, University of Nebraska - Lincoln, North Platte, Nebraska, USA

[4]Syngenta Crop Protection, Stein, Switzerland

[5]SimuTech Group, Toronto, Canada

Correspondence
Jonnie Dunne, Stone Environmental, 535 Stone Cutters Way, Montpelier, VT 05602, USA.
Email: jonnie@stone-env.com

Assigned to Associate Editor Gonzalo Martinez Garcia.

Abstract

Currently, the concept of plant capture efficiency is not quantitatively considered in the evaluation of off-target drift for the purposes of pesticide risk assessment in the United States. For on-target pesticide applications, canopy capture efficiency is managed by optimizing formulations or tank-mixing with adjuvants to maximize retention of spray droplets. These efforts take into consideration the fact that plant species have diverse morphology and surface characteristics, and as such will retain varying levels of applied pesticides. This work aims to combine plant surface wettability potential, spray droplet characteristics, and plant morphology into describing the plant capture efficiency of drifted spray droplets. In this study, we used wind tunnel experiments and individual plants grown to 10–20 cm to show that at two downwind distances and with two distinct nozzles capture efficiency for sunflower (*Helianthus annuus* L.), lettuce (*Lactuca sativa* L.), and tomato (*Solanum lycopersicum* L.) is consistently higher than rice (*Oryza sativa* L.), peas (*Pisum sativum* L). and onions (*Allium cepa* L.), with carrots (*Daucus carota* L.) showing high variability and falling between the two groups. We also present a novel method for three-dimensional modeling of plants from photogrammetric scanning and use the results in the first known computational fluid dynamics simulations of drift capture efficiency on plants. The mean simulated drift capture efficiency rates were within the same order of magnitude of the mean observed rates of sunflower and lettuce, and differed by one to two orders for rice and onion. We identify simulating the effects of surface roughness on droplet behavior, and the effects of wind flow on plant movement as potential model improvements requiring further species-specific data collection.

1 | INTRODUCTION

Applying pesticides in a manner that optimizes plant protection effectiveness and reduces off-target movement is a highly technical process that may be complicated by various

operational and environmental factors (Frankel, 1986; Nuyttens et al., 2006a; Nuyttens et al., 2006b). Research has shown that nozzle type, target crop growth habit, leaf surface roughness, wind speed, atmospheric turbulence, air temperature, and humidity can all affect pesticide capture efficiency, commonly measured as the area-normalized quantity of pesticide deposited on the target plant (Baker et al., 1983; Boize et al., 1976; Chowdhury et al., 2005; Sanyal et al., 2006). However, there is limited prior research focused on how these factors affect pesticide capture efficiency of spray drift for different off-target plant species. As such, nontarget organism exposure assessments for regulatory purposes typically assume that 100% of drift in the vicinity of nontarget plant species is captured by the canopy, and do not account for the unique physical properties of individual plant species or canopy types (Forster et al., 2012). Therefore, current guidance for determining spray drift buffers may lead to overestimation of the distance required to prevent off-target drift reception from exceeding effects thresholds. Improving the accuracy of models for quantifying the magnitude and subsequent implications of off-target pesticide transport via spray drift is critical to estimating ecological exposure and inferring potential impact on adjacent crops and non-target species. Thus, the primary goal of this research is to investigate variability of capture efficiency between plant species in the presence of drift spray droplets in order to improve understanding of off-target impacts of pesticides.

Another significant impediment in the advancement of regulatory models is that they are typically two dimensional. Two-dimensional modeling has been useful in predicting fate and transport in very specific conditions but cannot fully account for turbulent airflow that may be created in complex plant canopies, ambient wind conditions, sprayer fans (Hong et al., 2021), or emerging technologies such as applications from Unmanned Aircraft Systems. Modeling the effects of turbulent airflows on the fate and transport of pesticide particles has the potential to increase the accuracy of risk assessments and improve design of nontarget drift studies.

Perhaps the most promising tool for modeling turbulent airflows in pesticide applications is computational fluid dynamics (CFD). Generally, CFD uses numerical analysis to solve problems involving fluid flows. In the case of pesticide application studies, CFD is typically applied by dividing fluid domains into individual mesh cells and solving the Navier-Stokes equations for each cell for multiple iterations before the velocity and turbulence terms are resolved. To date, researchers have used three-dimensional (3D) modeling in CFD software to simulate entrained air currents, droplet release, turbulent air flows in plant canopies, and spray droplet retention on leaf surfaces (see Hong et al., 2021 for a full review). However, each of these elements can require enormous computational resources, and no research has yet combined them to model drift deposition on plants. The lack

> **Core Ideas**
>
> - Pesticide risk assessments assume complete capture of spray drift and in reality capture efficiency varies by species.
> - Capture efficiency is dependent on surface wettability and orientation.
> - Numerical models and digital photogrammetry can be used to simulate spray drift experiments.

of comprehensive models for drift deposition on plants is partially due to the difficulty of accurately modeling plant canopy geometry. Photogrammetric scanning has been used to triangulate key features that are used as the basis for building 3D plant models for other applications but has not yet been employed for CFD modeling. Photogrammetric scanning itself can be challenging due to self-occlusion by plant organs (Yan et al., 2014), small features that are difficult to photograph (Wen et al., 2018), and movement during the scanning process by plants that are variably rigid (Nguyen et al., 2016). The secondary goal of this research is to model variability in drift capture efficiency due to plant shape by using photogrammetric models in CFD modeling.

2 | METHODS

2.1 | Wind tunnel capture efficiency experiments

2.1.1 | Wind tunnel trials configuration

Area-normalized deposition on plants following spray applications were compared in an indoor wind tunnel in order to determine how capture efficiency varies by plant species. We calculated area-normalized deposition for all combinations of two nozzle types (air induction flat spray AIXR TeeJet 11003 and wide-angle flat spray TTI TeeJet 11003), two downwind distances (4.5 m, a distance used for vegetative filter strip placement and 7.6 m, used for no spray buffer distances for sensitive areas (Syngenta, 2013; USEPA, 2008; USEPA et al., 2020), and common cultivars of seven plant species grown to target heights between 10–20 cm and two–three leaves for onions (carrot—Nantes Coreless [*Daucus carota* L.], lettuce—Parris Island COS [*Lactuca sativa* L.], onion—Caribbean Garden Seeds Red Onion [*Allium cepa* L.], peas—Cascadia Sugar Snap [*Pisum sativum* L.], rice—RexRice [*Oryza sativa* L.], sunflower—AMS7110 Black Oil [*Helianthus annuus* L.], tomato—Quali T 47 [*Solanum lycopersicum* L.]). We completed six repetitions for each of the 14
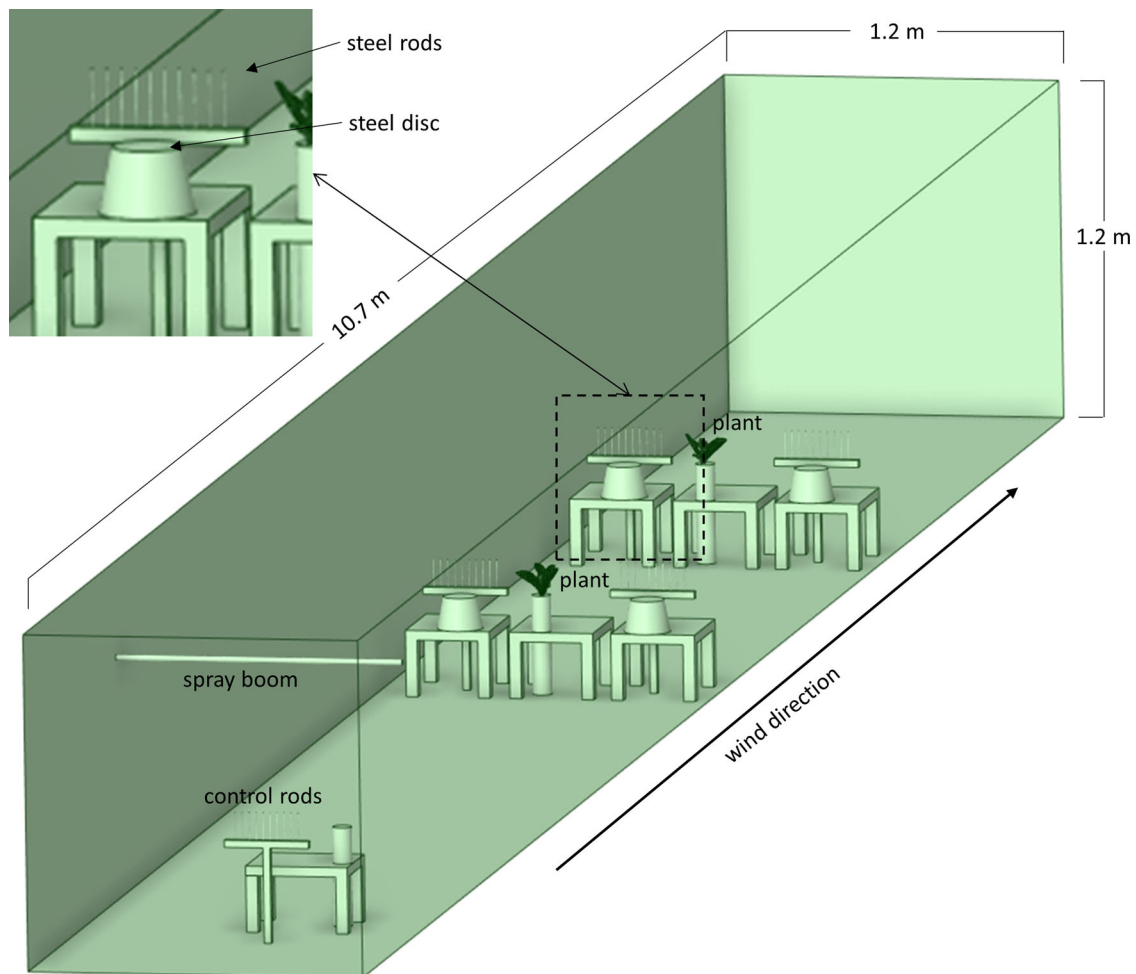
FIGURE 1 Wind tunnel schematic and simulation domain used in CFD modeling of spray trials. CFD, computational fluid dynamics.

combinations of plant species and nozzle in randomized order for a total of 84 trials, and each trial contained plants at both downwind distances.

The wind tunnel itself is located at the University of Nebraska Pesticide Application Technology (PAT) Laboratory in North Platte, NE and measured 10.7-m long, 1.2-m wide, and 1.2-m tall. Two nozzles vertically oriented toward the ground were spaced at 50 cm intervals on a spray boom, which was perpendicular to and centered across the wind tunnel width and 50 cm above spray drift receptors (Figure 1). The spray drift receptors at each downwind distance consisted of a single potted plant situated between two paired combinations of stainless-steel discs with 12-cm diameter and a stand containing 10 stainless-steel rods that were 10-cm long with 20-mm diameter. Stainless steel receptors were chosen as benchmarks for comparison to the deposition rates measured in plants since they are commonly used in drift deposition studies (Munjanja et al., 2020), with vertical rods known to have significantly higher capture efficiency than disks (Brain et al., 2019). An additional set of negative control rods was situated 90 cm upwind of the spray boom. All receptors,

including plants and stainless-steel instruments were held stable in plastic containers 37 cm above the ground surface. The plants were centered across the width of the wind tunnel, but due to the dimensions of the containers, the rods and discs on the left side facing downwind were 30 cm to the left of the plants, while those on the right were 37 cm to the right of the plants. This arrangement likely led to lateral variation in drift deposition for the rods and discs. Since the plants at the 7.6 m distance were sited directly downwind of the 4.5 m plant, it is expected that plants located at the 4.5 m distance may have intercepted droplets that would have moved to the 7.6 m receptors. Of course, in reality, these row crops are grown in larger and denser configurations, with each plant likely affecting the airflow and associated deposition of its neighbors. However, scoping studies showed that simulating airflow and deposition for a large cluster of plants is beyond our computational capacity. Therefore, we elected to isolate the shape of a single plant canopy and its surface characteristics as the explanatory variables for our studies of variability in drift capture efficiency. Here we also assume that the differences observed between species in drift capture efficiency are functions of differences

in plant characteristics and that these differences also exist in row crop formations, while recognizing that the magnitude of the differences would likely change to some degree.

2.1.2 | Spray application and recovery

Prior to spray application, air was pulled through the tunnel via fans until it reached a steady target wind speed of 4.5 m/s (∼10 mph). This speed was chosen as it is the upper limit of permitted wind speeds for applications of many pesticides (Kruger, 2018), and scoping studies showed that, for some plants, at lower wind speeds drift deposition was below the limit of quantification. A 3% aqueous suspension of *p*-toluene sulfonic acid tracer was then applied for 4 s at 2.76 bar during each trial. This pressure is recommended by the manufacturer as excellent for drift management, producing very coarse droplets for the AIXR nozzle and ultra-coarse droplets for the TTI nozzle. The target quantity of solution applied was 150 g, and the measured quantity applied averaged by species and nozzle was 148.1–151.5 g, with a maximum range of 7 g. Because the target application rate was not achieved during one AIXR lettuce trial and one AIXR rice trial they were excluded from further analysis. Following application, spray droplets were allowed to settle for 1 min before drift receptors were collected. The target temperature and relative humidity conditions were 20°C and 55%, respectively, and recorded at 1-min intervals during the trials.

The quantity of spray captured by the plants, rods, and discs was measured by rinsing the receptors with isopropanol and estimating the mass of the analytical tracer in the remaining solution via fluorescence spectrophotometry with an Ocean Optics Flame S spectrometer. Since mass was calculated as a product of fluorescence using linear regression modeling some of the calculations returned negative mass values. In these cases, the mass was assumed to be equal to the lowest reported positive value, 0.005 μg.

2.1.3 | Plant shape and surface characterization

Plants were grown indoors to a target maturity of 10- to 20-cm tall, or two–three leaves per plant for onions. The surface area of the plants was measured or modeled in a hierarchical fashion (Table 1). The primary and most accurate source was from 3D models completed for two plants each for rice, onion, sunflower, and lettuce in preparation for CFD modeling (see plant canopy model). When that was not available the secondary source was from flatbed scans of leaves for six plants randomly selected from all species. When neither measure was available for an individual plant, the third source was from calculating the ratio of surface area to dry

weight for the plants measured using the first two methods and multiplying the average ratio per species by the dry weight of the remaining plants.

Static contact angle measurements were taken at the PAT Laboratory using an OCA15EC optical contact angle goniometer manufactured by DataPhysics Instruments USA Corp. for each plant species by applying five drops of the spray solution on each of five tissue samples collected from the top, middle, and bottom of each species. These data provided information about the relative wettability of each of the species tested at the respective stage of growth.

2.1.4 | Statistical analysis

Differences in capture efficiency between plant species were evaluated through statistical comparisons of means, partitioned by plant species, nozzle, and downwind distance. Capture efficiency was calculated as area-normalized deposition of dye mass ($μg/cm^2$) for each receptor. Pairwise comparisons of means between all species were conducted using the independent *t*-test where the data were normally distributed (Shapiro-Wilk test, $α = 0.05$) and variance is equal (Levene's test, $α = 0.05$). When pairs did have normal distributions but did not have equal variance Welch's *t*-test was used. When they were not normally distributed the nonparametric Kruskal Wallis test was used ($α = 0.05$). We also conducted Kruskal Wallis tests for sets of the rods and discs, organized by species, distance, and nozzle as standards to test for any unintended variability in the quantity of drift present between trials.

2.2 | Computational fluid dynamics model formulation

2.2.1 | Atmospheric fluid model

The standard Shear Stress Transport k-ω model as implemented in Fluent (ANSYS, Inc., 2022a) was used to model airflow. This model solves the Reynolds-averaged Navier-Strokes equations by simplifying the Reynolds stresses into two turbulence quantities, k and ω. This has been shown to provide accurate and reliable calculations for a wide class of flows (ANSYS, Inc., 2022b). A no-slip condition was applied at the walls of the domain so that the airflow is limited to zero velocity in these areas. We also used a production limiter equation to limit excessive generation of turbulence energy in the vicinity of stagnation points (Menter, 1994).

A simulation domain was drafted to match the dimensions of the indoor wind tunnel (Figure 1). The downwind end of the wind tunnel was modeled as a mass-flow outlet boundary, with a mass flow rate of 8.1 kg/s which

TABLE 1 Mean surface area, mass, and surface area to mass ratios by species.

Species	Height (cm)	3D model surface area (cm^2)	Scanned surface area (cm^2)	Dry mass (g)	Surface area:mass	Model surface area (cm^2)
Carrot	10.9	–	43.2	0.05	659.8	31.1
Lettuce	13.9	470.2	602.0	0.65	817.1	532.0
Onion	30.8	81.8	57.4	0.12	536.1	59.8
Pea	16.3	–	152.2	0.22	754.7	167.9
Rice	17.5	11.9	9.5	0.02	749.6	10.8
Sunflower	19.9	366.7	294.7	0.51	520.5	262.4
Tomato	12.6	–	245.8	0.38	537.5	202.6

Note: Individual plant model surface area is first assigned 3D model surface area, then scanned surface area, then calculated from dry mass and mean species surface area:Mass if the other sources are not available. For height, $n = 12$, 3D model surface area $n = 2$, scanned surface area $n = 6$, dry mass $n = 24$.
Abbreviation: 3D, three-dimensional.

corresponds to the rate of airflow at the 4.5 m/s target wind speed across the wind tunnel inlet. The inlet was modeled as a pressure inlet boundary with 0 Pa gauge total pressure (i.e., at atmospheric pressure), flowing normal to the boundary. The turbulence is specified with a turbulent intensity of 0.5% calculated from 3D anemometer data collected at 1 s intervals for 10 min in the center of the inlet. We then selected a turbulent viscosity ratio (turbulent viscosity/fluid physical viscosity) of one which generally corresponds with equally low turbulence environments (Rumsey, 2019). Given the low turbulence of the wind tunnel air stream, and the high computational demands of simulating airflow around complex plant geometry, a pressure-based steady-state solution was calculated.

2.2.2 | Plant canopy model

We used digital photogrammetry scans of selected experimental plants to generate 3D plant canopy models for use in the CFD simulations. Given the time- and computationally-intensive nature of plant modeling and CFD simulations, we limited the modeling to two species each from the high and low capture efficiency groups, using the same plants that were used in a randomly selected AIXR trial. We selected plants from the AIXR trials since early scoping experiments had shown that the magnitude of the residues on the plants would likely be higher for this nozzle and less sensitive to experimental noise (Padilla et al., 2018), and comparisons of mean plant height between nozzles (Welch's *t*-test, $\alpha = 0.05$) showed no significant variation. We found that modeling carrot geometry was not feasible since photogrammetric scans of the very fine leaves yielded insufficient data for reconstructing the plant canopy.

We used an EinScan Pro 2X photogrammetric scanner manufactured by Shining 3D, to generate 3D point clouds of the selected plants at the PAT Laboratory immediately before spray application, and used Meshlab (Cignoni et al., 2008) to convert the point clouds into watertight models of the
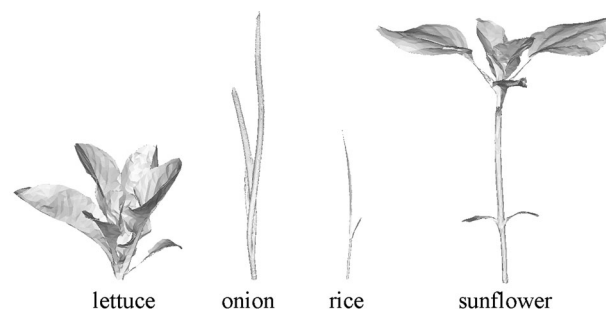

lettuce   onion   rice   sunflower

FIGURE 2 Examples of plant models derived from digital photogrammetry scans and used in CFD modeling. CFD, computational fluid dynamics.

plants suitable for use in CFD modeling (Figure 2). The point clouds were of very high resolution (0.2 mm minimum sample distance) and accuracy (0.05 mm). However, models of plants in the size range of the experimental plants generated from a point cloud with these qualities would consist of millions of small faces. This would be problematic in CFD simulations of our experiments, in which the fluid domain of the wind tunnel must first be discretized into a 3D mesh, comprised of faces that correspond to the size and shape of the plant models at the plant-volume interface. Beginning with extremely small plant faces results in highly distorted volume mesh elements which are numerically unstable in the CFD solver. Extremely small plant faces also result in an excessive number of mesh elements, leading to unreasonably long simulation times in the CFD solver. As such, the initial point clouds were first subsampled to a 0.5 mm sample distance, and initial surfaces were generated using the ball pivoting algorithm with a 0.5 mm radius (Bernadini et al., 1999). For the lettuce, sunflower, and rice models, the flattened leaves were then separated from the stems, offset to match the mean thickness of leaves measured on site throughout the plants ($n = 6$), and reattached to the stems. The initial watertight models varied in size by species: lettuce ~4 million, sunflower ~3 million, rice ~300k, onion ~60k. Through iterative testing we found that the resulting watertight models ultimately needed to be

simplified to approximately 8000 faces per plant in order for the sizes of the faces to be large enough that they could be used to successfully generate a stable volume mesh. Some regions of the plant surfaces were either occluded from the scanner, too glossy to be triangulated, or formed features that were too small to register in multiple images. In these cases, reference photos of the plants were used to manually edit the meshes to match the shapes of the plant subjects. We also recorded the approximate orientation of the plants as they were placed in the wind tunnel and replicated that orientation in the CFD models.

2.2.3 | Droplet spray and deposition model

Injection profiles were generated from spray droplet velocity and dimension data collected at the West Jefferson, Ohio Battelle campus with an VisiSize P15 particle size analyzer manufactured by Oxford Lasers and used to simulate spray applications in the CFD models. For each nozzle, the instrument took measurements by scanning the entire width of the spray plume 165 mm below the nozzle while spraying water at 2.76 bar, the same pressure used in the experimental trials. This process was repeated in triplicate while ensuring that sufficient droplets (average 25,000 per replicate) were measured in order to provide accurate size and velocity data. The nozzle spray droplet size data showed that the AIXR nozzle produced droplets with average Dv10, Dv50, and Dv90 (10%, 50%, and 90% of the spray volume contains droplets smaller than the specified diameter, respectively) of 142, 389, and 646 μm, respectively, with 10.2% of the droplets (by volume) under 141 μm. The AIXR nozzle produced finer droplets than the TTI nozzle for which the average Dv10, Dv50, and Dv90 were 319, 758, and 1284 μm, respectively, and 1.7% of the droplets (by volume) were under 141 μm. These droplet size distributions are consistent with approximate figures provided by the manufacturer.

During spray application simulation, discrete liquid droplets are released into a continuous airflow. The droplets are modeled as inert, rotating, ellipsoidal point mass particles with sphericity derived from spray characterization data (0.88 for AIXR, 0.91 for TTI) and used to calculate nonspherical drag coefficients (Haider & Levenspiel, 1989). The droplet size and velocity distributions of the simulated spray applications are generated from spray characterization data to replicate 1 s of the measured flow rates of each nozzle. Droplets are released into the airflow from random positions within an ellipse located 165 mm below the spray boom (matching the distance from nozzle where the spray has been measured). Droplets are also constrained to match the 110° width and 6° depth of the fan-shaped sprays produced by the AIXR and TTI nozzles. The simulated deposition is then multiplied by four to match the 4 s duration of the

experimental trials. Stochastic tracking of particle paths was used, including a discrete random walk model. These incorporate the random effects of local turbulence velocity on particle dispersion by including the instantaneous value of the fluctuating gas flow velocity in addition to the mean fluid phase velocity in predictions of particle trajectories (ANSYS, Inc., 2022b). The trajectory is computed in this manner for a representative number of particles (here we specified 20 particles and the default time constant of 0.15) to determine the random effects of turbulence which are then applied to particle dispersion. The limits of this model include the fact that variability in plant surface characteristics is not modeled, so droplets that collide with any surface are assumed to be fully trapped, when in reality droplets are known to bounce or shatter during impaction, and that the droplets will not interfere with one another. For each plant species, replicates of the deposition trials were simulated by applying the three separate injection profiles for each of the two nozzles to the same set of two 3D plant models. We then calculated the model bias as the ratio of the modeled deposition averaged by species, nozzle, and distance to the observed deposition averaged by species, nozzle, and distance.

3 | RESULTS AND DISCUSSION

3.1 | Wind tunnel capture efficiency experiments

Statistical comparisons of observed area-normalized means in drift capture efficiency show that across nozzles and distances there are statistically significant differences in most comparisons. Observed capture efficiency summarized by species, nozzle, and distance is presented in Figure 3. Species summaries are ordered high to low by mean deposition observed in the AIXR 4.5 m measurements, and statistically distinct species are labelled by letters. Generally, there appear to be two distinct groups of plants: those with high capture efficiency (tomato, sunflower, lettuce, carrot), and those with low capture efficiency with some variance between members of the group (pea, rice, onion). As expected, discs show capture efficiency that falls between the two groups and the rods show the highest drift capture efficiency (Brain et al., 2019). Ellis et al. (2018) postulated that based on the plant's shape, size, and movement in wind, collection efficiency of plants would be lower than the vertical rods. Ellis and co-authors stated that the vertical rods were designed to be relatively efficient in capturing airborne sprays (~80%).

The high degree of control of operational parameters for the spray applications and the consistency in the variability of capture efficiency between species across nozzle types and downwind distances, indicates that the observed variability is due to the characteristics of the receptors themselves. The
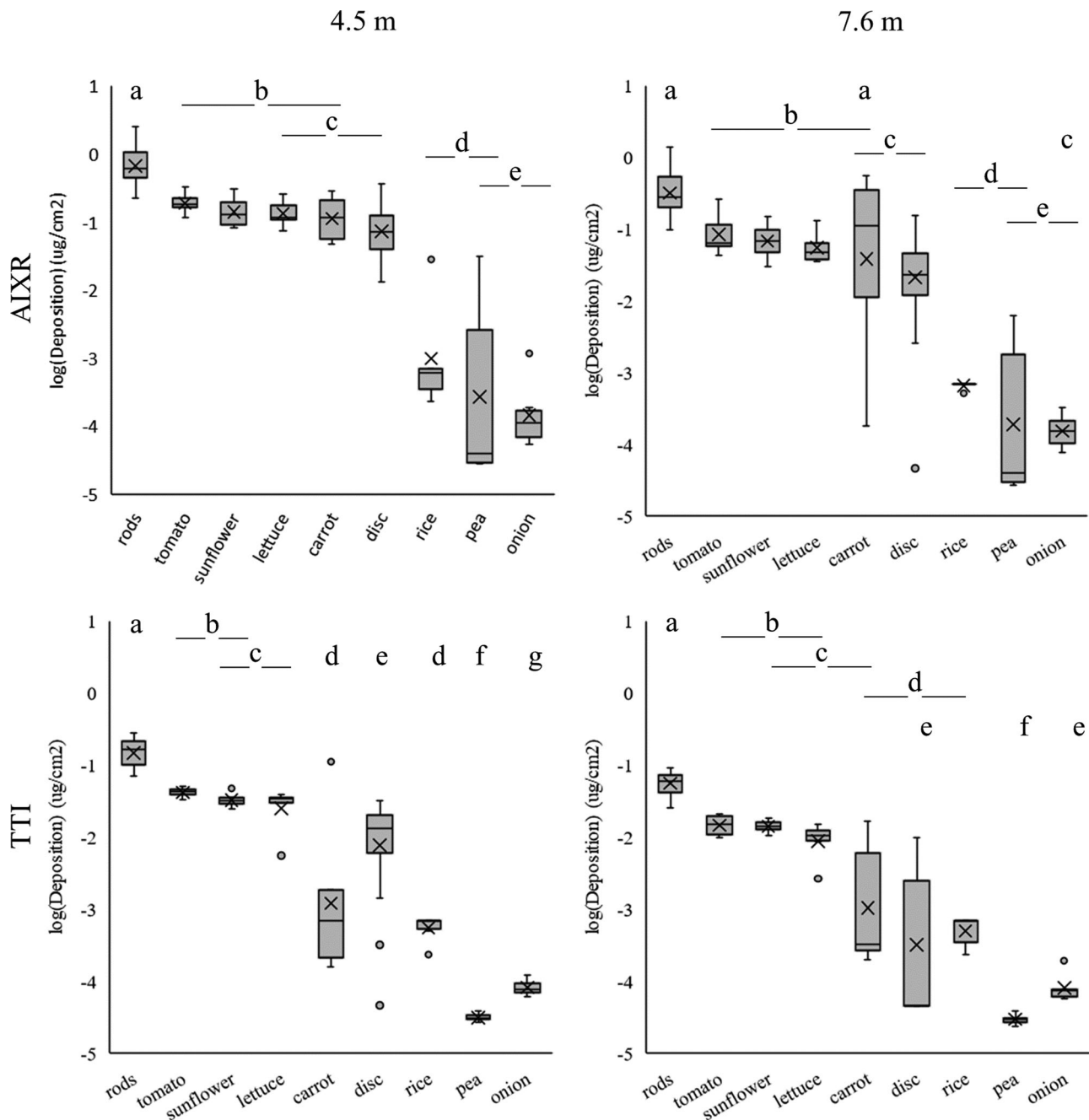
FIGURE 3 Comparisons of mean area-normalized drift deposition from wind tunnel experiments. Letters denote statistically significant difference of means between groups, mean is symbolized as *X*, whiskers extend to 1.5 times the interquartile range. For each comparison, independent *t*-tests are used when datasets are normally distributed (Shapiro–Wilk test), and variance is equal (Levene's test). If variance is not equal, Welch's *t*-test is used. If data are not normally distributed, the Kruskal–Wallis *H* test is used. $\alpha = 0.05$ for all tests and $n = 6$ for each trial.

analysis of variance of deposition on rods and discs between species, partitioned by nozzle and distance, showed no significant variance, the measured quantity of spray solution released did not vary by more than 4%, and no solution was detected on the control rods. Meteorological conditions were also stable between trials; temperature and relative humidity (RH) values averaged by species and nozzle were 20.9–21.1°C and 54%–55% RH.

It appears that the primary sources of the variability in capture efficiency between receptors are surface characteristics and receptor shape. The orientation and roughness of the leaves are known to be important since they have been shown to affect whether droplets adhere, bounce, or shatter when impacting plant surfaces (Delele et al., 2016). Previous research has shown low capture efficiency of on-target spray applications being associated with low wettability (Fang et al.,
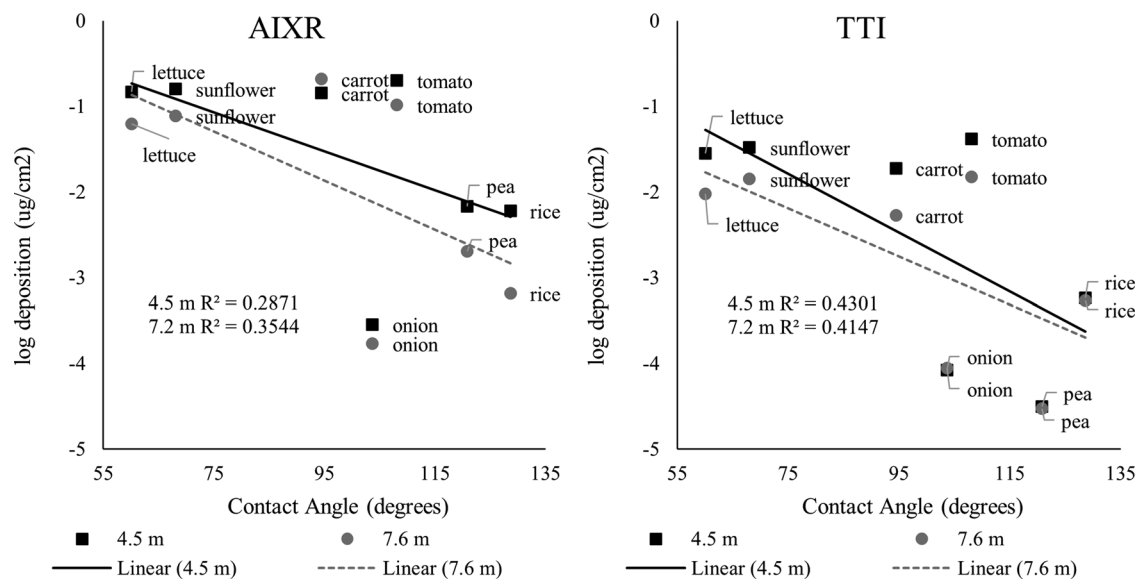
FIGURE 4 Relationship between average species contact angle ($n = 25$) and log of area-normalized deposition ($n = 6$).

2019; Wei et al., 2020). Our results are consistent with those findings, the plants that showed low drift capture efficiency also had low wettability (indicated by high contact angles: onion 103°, pea 120°, and rice 128°). Except for tomatoes, the plants with high deposition also showed higher wettability based on lower contact angles (lettuce 60°, sunflower 68°, and carrot 94°). The low capture efficiency plants are also notable for having narrow or fine leaves and stems that were observed to bend and sway significantly during the wind tunnel capture efficiency experiments, conforming to the airflow direction. In contrast the high capture efficiency plants have larger leaves and stiffer stems likely had more surface area that was not oriented with the wind flow direction. The high capture efficiency observed in the steel rods relative to the steel discs also illustrates the effect of vertical orientation resulting in greater capture efficiency. The tendency of capture efficiency to be responsive to contact angles is illustrated here through regression analyses which show consistent mid-level coefficients of determination across nozzles and downwind distances (Figure 4). Some of the error in these regression analyses is likely due to difference in plant canopy shape factors such as leaf orientation. Note that these results show the tomato plants with high capture efficiency, despite the measured contact angle being greater than 90°, which has been reported as the transition point beyond which wettability declines (Tanaka et al., 2014). However, these contact angle values for tomato plants are approximately 20° greater than when measured with water alone (Fernandes et al., 2014) and are approximately 60° greater than when measured in a similar previous scoping study (Dunne et al., 2020).

The observed variability of drift capture efficiency is an important factor that should be considered in regulatory modeling. Without accounting for the characteristics of plants that

reduce drift capture efficiency, regulators are possibly overestimating the magnitude of drift exposure and its effects. Furthermore, given the basic knowledge of the relationships between plant characteristics and drift capture efficiency, it appears that further research investigating a wider range of plant types could potentially yield predictive models that could be extended to other crops and endangered species risk assessments.

3.2 | CFD simulation of capture efficiency

Modeled deposition was typically within an order of magnitude of observed deposition across species, nozzles, and downwind distances. The most significant exception is for the steel discs, where the model showed no deposition except at 15 ft during the TTI trials. Model bias of the CFD simulations of drift capture efficiency is presented in Table 2. The data for rods and discs are reported by lateral position since they were not evenly spaced across the width of the wind tunnel and varied in deposition. Note that the variability in deposition between replicates of CFD simulations is due solely to differences in the three replicates of spray characterization data used in modeling, whereas the shape and orientation of the plant canopies varied somewhat between replicates of the experimental trials. This is a shortcoming of the model that could be improved upon in future work, potentially by simply rotating the plant models or using numerous individual plant models, but doing so requires generating new meshes, solutions, and particle trajectories each time.

While other studies have successfully simulated drift deposition using CFD on manufactured receptors such as filter paper (Baetens et al., 2007), or rods and pipe cleaners within

TABLE 2 Results of the CFD simulations of drift capture efficiency.

Receptor	Position	Distance (m)	Model bias AIXR	TTI
Disc	Left	4.5	0.00	27.26
	Right	4.5	0.00	0.52
	Left	7.6	0.00	0.00
	Right	7.6	0.00	0.00
Rods	Left	4.5	4.83	33.41
	Right	4.5	5.93	42.07
	Left	7.6	5.97	31.25
	Right	7.6	4.51	18.97
Lettuce		4.5	0.23	1.21
		7.6	0.29	1.31
Onion		4.5	60.67	230.70
		7.6	78.79	123.05
Rice		4.5	9.06	198.12
		7.6	59.00	52.28
Sunflower		4.5	0.15	1.24
		7.6	0.20	0.69

Note: Model bias, mean modeled/mean observed. $n = 3$ for modeled and $n = 6$ for observed.

Abbreviation: CFD, computational fluid dynamics.

or near tree canopies (Duga et al., 2017; Endalew et al., 2010; Endalew et al., 2011; Hong et al., 2018), this is the first time to our knowledge that deposition on entire plants has been directly simulated and validated. While the aforementioned studies did show better agreement for the receptors they studied, they also showed model bias that varied with operational factors such as nozzle type and distance from nozzle. The results found in these studies indicate that while the CFD modeling framework has the potential to provide researchers with the capacity to rapidly and accurately explore numerous combinations of spray drift experimental variables, more work is needed to develop stable models of drift deposition.

The species showing higher than observed drift capture efficiency, onion and rice, are both species that showed low drift capture efficiency in the wind tunnel experiments and low wettability from contact angle measurements. The opposite holds true for lettuce and sunflower, which showed relatively higher deposition in the experimental trials, lower than observed modeled deposition for the AIXR nozzle, and high wettability. For onion and rice the high model bias is likely due to the following factors: (1) the modeled plants are inert and did not bend as they did during experiments, and (2) all droplets impacting the plant surface are assumed to be deposited. In reality, the wind bent the onion and rice so that the leaf surfaces were oriented with the airflow, which would increase the angle of incidence and reduce the likelihood that a droplet adheres to the plant surface. In contrast,

the low model bias of the sunflower may be due to the fact that during the experimental trials, bending in the wind may have increased drift capture efficiency when flat and level leaves bent and had their undersides exposed, creating turbulence and low incidence angles with impacting droplets. In addition, the low wettability of the onion and rice indicates that some of the droplets would have bounced during the experimental trials, and this process was not modeled. While it is possible to simulate the fluid-structure interaction between airflow and branches/leaves (Duga et al., 2014), this type of modeling has not been validated with field observations. Measurements of the required inputs for plants (Young's modulus and Poisson's ratio) is also challenging and was beyond the scope of this work. It is similarly possible to model droplet bouncing and shattering if surface roughness is known (Delele et al., 2016) but measuring the surface roughness, which will vary throughout the plant, is difficult. Modeling surface-droplet and fluid-structural interactions are also computationally expensive, and the simulations of deposition and plant shape alone required all available processing power (a single workstation with 32GB RAM, Intel Core i7-7700K CPU @ 4.20 GHz, 4 cores), and approximately 8 h to solve. The high computational demands are due largely to the complex nature of the meshes built around the intricate plant shapes. The number of cells for each species is as follows: onion—3 million, rice—5 million, lettuce—5.6 million, sunflower—9.7 million. Although creating and solving these simulations is onerous, once they are improved by integrating surface-droplet and fluid-structural interactions, expanding the simulation domain to rows of multiple crops and stages, and solved for multiple wind speeds and directions, they could potentially be compiled as standalone applications. We envision that users could then provide updated spray characterization data to evaluate the effects of new spray technology without needing to model additional plants or fluid flows.

4 | SUMMARY AND CONCLUSIONS

This work has shown that drift capture efficiency varies between plant species across different nozzle types and downwind distances. It is also notable that all species studied show lower capture efficiency than steel rods which are commonly used in regulatory drift studies (several species also showed lower capture efficiency than steel discs). Accounting for this variability in capture efficiency could become an element of regulatory drift modeling, resulting in risk assessments that more accurately reflect and bracket drift exposure conditions. Future research that replicated this work with a wider variety of plant species and quantitative analysis of the effects of plant surface and shape characteristics on drift capture efficiency could potentially yield predictive models of drift capture effi-

ciency. This would be of particular value when attempting to study the risks posed to endangered plants.

This work has also shown that modeling the effects of nozzle type, downwind distance, and plant shape on drift deposition on plants is possible using CFD given the observed variability in model bias across species. We also recommend that methods to model droplet-surface interactions and fluid-plant interactions be further developed and incorporated into the CFD simulations we have developed. This research for example could be improved by modeling multiple sets of plant models per species to better account for variability in plant shape. Novel combinations of adjuvants, nozzle types, and plant types require better understanding of the risk for adverse effects to off-target plant species from spray drift deposition and CFD has been shown to be useful in exploring the implications of a multitude of possible configurations.

AUTHOR CONTRIBUTIONS

Jonnie Dunne: Data curation; formal analysis; investigation; methodology; project administration; resources; software; visualization; writing–original draft; writing–review and editing. **Shanique Grant**: Conceptualization; funding acquisition; investigation; methodology; project administration; resources; supervision; writing–review and editing. **Jeffrey Golus**: Investigation; methodology; resources; supervision. **Jeffrey Perine**: Conceptualization; methodology. **Stefan Wolf**: Conceptualization; investigation; methodology; resources. **Michael Winchell**: Supervision. **Mark Ledson**: Conceptualization; data curation; investigation; methodology; resources. **Ian Whenham**: Methodology.

ACKNOWLEDGMENTS

CONFLICT OF INTEREST STATEMENT

The authors declare no conflicts of interest.

ORCID

Jonnie B. Dunne https://orcid.org/0000-0001-5572-4282
Shanique L. Grant https://orcid.org/0000-0001-6152-237X

REFERENCES

ANSYS, Inc. (2022a). *Fluent 2022 (R1)* [computer software]. https://www.ansys.com/products/fluids/ansys-fluent

ANSYS, Inc. (2022b). *Fluent theory guide*. Ansys. https://ansyshelp.ansys.com/account/secured?returnurl=/Views/Secured/corp/v221/en/flu_th/flu_th.html

Baetens, K., Nuyttens, D., Verboven, P., De Schampheleire, M., Nicolaï, B., & Ramon, H. (2007). Predicting drift from field spraying by means of a 3D computational fluid dynamics model. *Computers and Electronics in Agriculture*, *56*(2), 161–173. https://doi.org/10.1016/j.compag.2007.01.009

Baker, E. A., Hunt, G. M., & Stevens, P. J. G. (1983). Studies of plant cuticle and spray droplet interactions: A fresh approach. *Pesticide Science*, *14*(6), 645–658. https://doi.org/10.1002/ps.2780140613

Bernardini, F., Mittleman, J., Rushmeier, H., Silva, C., & Taubin, G. (1999). The ball-pivoting algorithm for surface reconstruction. *IEEE Transactions on Visualization and Computer Graphics*, *5*(4), 349–359. https://doi.org/10.1109/2945.817351

Boize, L., Gudin, C., & Purdue, G. (1976). The influence of leaf surface roughness on the spreading of oil spray drops. *Annals of Applied Biology*, *84*(2), 205–211. https://doi.org/10.1111/j.1744-7348.1976.tb01749.x

Brain, R., Goodwin, G., Abi-Akar, F., Lee, B., Rodgers, C., Flatt, B., Lynn, A., Kruger, G., & Perkins, D. (2019). Winds of change, developing a non-target plant bioassay employing field-based pesticide drift exposure: A case study with atrazine. *Science of the Total Environment*, *678*, 239–252. https://doi.org/10.1016/j.scitotenv.2019.04.411

Chowdhury, A. B. M. N. U., Jepson, P. C., Ford, M. G., & Frampton, G. K. (2005). The role of cuticular waxes and surface roughness in determining the insecticidal efficacy of deltamethrin and dimethoate applied as emulsifiable concentrates to leaf surfaces. *International Journal of Pest Management*, *51*(4), 253–263. https://doi.org/10.1080/09670870500404674

Cignoni, P., Callieri, M., Corsini, M., Dellepiane, M., Ganovelli, F., & Ranzuglia, G. (2008). Meshlab: An open-source mesh processing tool. In *Eurographics Italian chapter conference* (pp. 129–136). The Eurographics Association.

Delele, M. A., Nuyttens, D., Duga, A. T., Ambaw, A., Lebeau, F., Nicolai, B. M., & Verboven, P. (2016). Predicting the dynamic impact behaviour of spray droplets on flat plant surfaces. *Soft Matter*, *12*(34), 7195–7211. https://doi.org/10.1039/C6SM00933F

Duga, A. T., Defraeye, T., Nicolai, B., & Verboven, P. (2014). Modeling air flow around branches and leaves using fluid-structure interaction simulations. *Aspects of Applied Biology*, *122*, 315–322.

Duga, A. T., Delele, M. A., Ruysen, K., Dekeyser, D., Nuyttens, D., Bylemans, D., Nicolai, B. M., & Verboven, P. (2017). Development and validation of a 3D CFD model of drift and its application to air-assisted orchard sprayers. *Biosystems Engineering*, *154*, 62–75. https://doi.org/10.1016/j.biosystemseng.2016.10.010

Dunne, J. B., Grant, S., Wolf, S., Perine, J., Ledson, M., Addison, D., Crane, J., & Winchell, M. (2020). *Modelling off-target plant canopy interception and retention of pesticide spray droplets* [*Conference* presentation]. American Chemical Society Fall 2020 Virtual Meeting. https://www.morressier.com/o/event/5f510f8733e12ddac138e635/article/5f511d216fdcfc687198b2db

Ellis, M. B., Brain, R. A., Perine, J. W., Cooke, C., Harrington, P., Lane, A. G., Lane, A. G., O'Sullivan, C. M., & Ledson, T. M. (2018). The importance of field-based drift exposure to biological outcomes: A novel case study with mesotrione. *Aspects of Applied Biology*, *137*, 317–323.

Endalew, A. M., Debaer, C., Rutten, N., Vercammen, J., Delele, M. A., Ramon, H., Nicolaï, B. M., & Verboven, P. (2010). Modelling pesticide flow and deposition from air-assisted orchard spraying in orchards: A new integrated CFD approach. *Agricultural and Forest Meteorology*, *150*(10), 1383–1392. https://doi.org/10.1016/j.agrformet.2010.07.001

Fang, H., Zhang, Z., Xiao, S., & Liu, Y. (2019). Influence of leaf surface wettability on droplet deposition effect of rape leaves and their correlation. *Journal of Agriculture and Food Research*, *1*, 100011. https://doi.org/10.1016/j.jafr.2019.100011

Fernandes, P. É., São José, J. F. B., Zerdas, E. R. M. A., Andrade, N. J., Fernandes, C. M., & Silva, L. D. (2014). Influence of the hydrophobicity and surface roughness of mangoes and tomatoes on the adhesion of Salmonella enterica serovar Typhimurium and evaluation of cleaning procedures using surfactin. *Food Control*, *41*, 21–26. https://doi.org/10.1016/j.foodcont.2013.12.024

Forster, W. A., Mercer, G. N., & Schou, W. C. (2012). Spray droplet impaction models and their use within AGDISP software to predict retention. *New Zealand Plant Protection*, *65*, 85–92. https://doi.org/10.30843/nzpp.2012.65.5393

Frankel, H. (1986). Pesticide application: Technique and efficiency. In J. Palter & R. Ausher (Eds.), *Advisory work in crop pest and disease management* (pp. 132–160). Springer.

Haider, A., & Levenspiel, O. (1989). Drag coefficient and terminal velocity of spherical and nonspherical particles. *Powder Technology*, *58*(1), 63–70. https://doi.org/10.1016/0032-5910(89)80008-7

Hong, S.-W., Park, J., Jeong, H., Lee, S., Choi, L., Zhao, L., & Zhu, H. (2021). Fluid dynamic approaches for prediction of spray drift from ground pesticide applications: A review. *Agronomy*, *11*(6), 1182. https://doi.org/10.3390/agronomy11061182

Hong, S.-W., Zhao, L., & Zhu, H. (2018). CFD simulation of pesticide spray from air-assisted sprayers in an apple orchard: Tree deposition and off-target losses. *Atmospheric Environment*, *175*, 109–119. https://doi.org/10.1016/j.atmosenv.2017.12.001

Kruger, G. (2018). *Strategies for managing pesticide spray drift* [Webinar]. USEPA. https://www.epa.gov/reducing-pesticide-drift/strategies-managing-pesticide-spray-drift-webinar-materials

Melese Endalew, A., Debaer, C., Rutten, N., Vercammen, J., Delele, M. A., Ramon, H., Nicolaï, B. M., & Verboven, P. (2011). Modelling the effect of tree foliage on sprayer airflow in orchards. *Boundary-Layer Meteorology*, *138*(1), 139–162. https://doi.org/10.1007/s10546-010-9544-6

Menter, F. R. (1994). Two-equation eddy-viscosity turbulence models for engineering applications. *AIAA Journal*, *32*(8), 1598–1605. https://doi.org/10.2514/3.12149

Munjanja, B. K., Naudé, Y., & Forbes, P. B. C. (2020). A review of sampling approaches to off-target pesticide deposition. *Trends in Environmental Analytical Chemistry*, *25*, e00075. https://doi.org/10.1016/j.teac.2019.e00075

Nguyen, C. V., Fripp, J., Lovell, D. R., Furbank, R., Kuffner, P., Daily, H., & Sirault, X. (2016). 3D scanning system for automatic high-resolution plant phenotyping. *2016 International conference on digital image computing: Techniques and applications (DICTA)* (pp. 1–8). IEEE.

Nuyttens, D., De Schampheleire, M., Steurbaut, W., Baetens, K., Verboven, P., Nicolai, B., Ramon, H., & Sonck, B. (2006a). Experimental study of factors influencing the risk of drift from field sprayers, Part 1: Meteorological conditions. *Aspects of Applied Biology*, *77*(2).

Nuyttens, D. D., De Schampheleire, M., Steurbaut, W., Baetens, K., Verboven, P., Nicolai, B., Ramon, H., & Sonck, B. (2006b). Experimental study of factors influencing the risk of drift from field sprayers Part 2: Spray application technique. *Aspects of Applied Biology*, *77*(2), 331–339.

Padilla, L., Grant, S., Dunne, J. B., Perine, J., & Ledson, M. (2018). Computational fluid dynamics modelling for plant canopy interception of pesticide spray droplets. *American Chemical Society Meeting & Exposition 256*, Boston, MA, United States.

Rumsey, C. (2019). *Turbulence modeling resource*. https://turbmodels.larc.nasa.gov/index.html

Sanyal, D., Bhowmik, P. C., & Reddy, K. N. (2006). Influence of leaf surface micromorphology, wax content, and surfactant on primisulfuron droplet spread on barnyardgrass (*Echinochloa crus-galli*) and green foxtail (*Setaria viridis*). *Weed Science*, *54*(4), 627–633. https://doi.org/10.1614/WS-05-173R.1

Syngenta. (2013). *6198 Actara-7lb.8oz.booklet.indd*. https://www.syngenta-us.com/current-label/actara

Tanaka, T., Lee, J., & Scheller, P. R. (2014). Interfacial free energy and wettability. In S. Seetharaman (Ed.), *Treatise on process metallurgy* (pp. 61–77). Elsevier.

USEPA. (2008). https://www.epa.gov/sites/default/files/2015-08/documents/epapyrethroidletter.pdf

USEPA. (2020). *Pesticide product label, Versys Insecticide*. https://www3.epa.gov/pesticides/chem_search/ppls/007969-00389-20201014.pdf

Wei, J., Tang, Y., Wang, M., Hua, G., Zhang, Y., & Peng, R. (2020). Wettability on plant leaf surfaces and its effect on pesticide efficiency. *International Journal of Precision Agricultural Aviation*, *3*(1). https://doi.org/10.33440/j.ijpaa.20200301.62

Wen, W., Zhao, C., Guo, X., Wang, Y., Du, J., & Yu, Z. (2018). Construction method of three-dimensional model of maize colony based on t-distribution function. *Transactions of the Chinese Society of Agricultural Engineering*, *34*(4), 192–200.

Yan, F., Sharf, A., Lin, W., Huang, H., & Chen, B. (2014). Proactive 3D scanning of inaccessible parts. *ACM Transactions on Graphics (TOG)*, *33*(4), 1–8.